Nuclear Instruments and Methods in Physics Research A 355 (1995) 3–18

NUCLEAR INSTRUMENTS & METHODS IN PHYSICS RESEARCH Section A

ELSEVIER

Principles of photon colliders

Valery Telnov *

Institute of Nuclear Physics 630090, Novosibirsk, Russian Federation

Abstract

Future linear colliders offer unique opportunities to study $\gamma\gamma$, γe interactions. Using the laser backscattering method one can obtain $\gamma\gamma$, γe colliding beams with energy and luminosity comparable to the electron–position luminosity or even higher. In this review physical principles of photon colliders are described and various problems, concerning the accelerator, laser, interaction region and luminosity are discussed. Some examples of physical processes are given.

1. Introduction

Since 1970 two-photon physics has been actively studied at e^+e^- storage rings in collisions of virtual photons. Their spectrum is $dn \sim 0.035 d\omega/\omega$, so that two-photon luminosity is much lower than that in e^+e^- collisions. Nevertheless, these experiments have given us a lot of information on the nature of elementary particle

Future linear colliders which are being developed now (see Table 1) offer unique, much more rich than before, opportunities to study $\gamma\gamma$ and γe interactions. Unlike the situation in storage rings, in linear colliders each bunch is used only once. This makes it possible to "convert" electron to high energy photons to obtain colliding $\gamma\gamma$ and γe beams. This idea was proposed by the author and colleagues in 1981 [1] and was further discussed and developed in Refs. [2–8,10]. Among various methods of $e \to \gamma$ conversion [7] the best one is Compton scattering of laser light on high energy electrons. This method is well known [9]. After scattering, the photons have an energy close to that of the initial electrons and follow their directions. The small bunch size in linear colliders makes it possible to achieve a conversion coefficient $k \equiv N_\gamma/N_e \sim 1$ at a moderate laser flash energy of a few joules. In $\gamma\gamma$ collisions a luminosity higher than in e^+e^- collisions is possible due to the absence of some collision effects. Monochromaticity of collisions near $\Delta W_{\gamma\gamma}/W_{\gamma\gamma} \sim 10\%$ can be obtained. Photons may have various polarizations, which is very advantageous for experiments.

The detailed considerations of the conversion, photon spectra and monochromatization of collisions can be found in Ref. [3]. Polarization effects have been considered in Ref. [6]. Collision effects restricting the luminosities, schemes of the interaction region, requirements for accelerators, attainable luminosities and other aspects of obtaining $\gamma\gamma$, γe collisions have been considered in Refs. [7,8]. Physical problems, which can be studied in $\gamma\gamma$, γe collisions, were discussed in many papers (see Refs. [10–14] and references therein).

Very rich physics, potentially higher than e^+e^- collisions luminosity, and simplification of the collider (positrons are not required) are all attractive to physicists. The progress in the development of high power lasers (both conventional and free-electron lasers) makes it now possible to seriously consider photon colliders.

2. Linear colliders

It is well known that due to the synchrotron radiation problem in e^+e^- storage rings the energy region beyond LEP II can only be explored by linear colliders. In linear colliders beams are used only once which opens the possibility to obtain $\gamma\gamma$, γe colliding beams.

With an achieved accelerating gradient of about 100 MeV/m and a reasonable length of 10–20 km the next linear colliders can cover the energy region up to 1–2 TeV which is comparable with the constituent energy potentially available at LHC. Due to the complexity of the task, the linear collider community is considering now as a first step a linear collider with a c.m. energy up to 500 GeV with a yearly integrated luminosity of about 20 fb^{-1}. Table 1 gives some parameters essential for out task of linear colliders now under consideration [15].

Beam parameters in the table have been optimized for e^+e^- collisions but may be used as a reference point for photon colliders.

* E-mail telnov@inp.nsk.su.

SSDI 0168-9002(94)01173-7

3. Backward Compton scattering, main characterictics of photon beams and γγ, γe collisions

If laser light is scattered off an electron beam, the photons after scattering have a high energy ($\omega \sim E_0$) and follow the initial electron direction with additional angular spread $\sim 1/\gamma$. This method of $e \to \gamma$ conversion has obvious advantages in comparison with other methods (bremsstrahlung on amorphous or crystal target, beamstrahlung during collision of e^+e^- beams) because of much better background conditions, the possibility of monochromatization ($\sim 10\%$ in $\gamma\gamma$ collisions and even better in γe collisions) and a high degree of circular polarization.

3.1. Kinematics

Below, formulae for Compton scattering are given for the case of our interest [3].

In the conversion region a photon with energy ω_0 is scattered on an electron with energy E_0 at a small collision angle α_0 (Fig. 1). The energy of the scattered photon ω depends on its angle ϑ relative to the motion of the incident electron as follows:

$$\omega = \frac{\omega_0}{1 + (\vartheta/\vartheta_0)^2}, \tag{1}$$

where

$$\omega_m = \frac{x}{x+1}E_0;$$

$$\vartheta_0 = \frac{mc^2}{E_0}\sqrt{x+1};$$

$$x = \frac{4E_0\omega_0\cos^2\alpha_0/2}{m^2c^4} \simeq 15.3\left[\frac{E_0}{\text{TeV}}\right]\left[\frac{\omega_0}{\text{eV}}\right],$$

where ω_m is the maximum photon energy.

For example: $E_0 = 300$ GeV, $\omega_0 = 1.17$ eV (neodinium glass laser) $\Rightarrow x = 5.37$ and $\omega/E_0 = 0.84$. As will be explained below, the value $x = 4.8$ is optimum for photon colliders; therefore further examples will be given for this value of x.

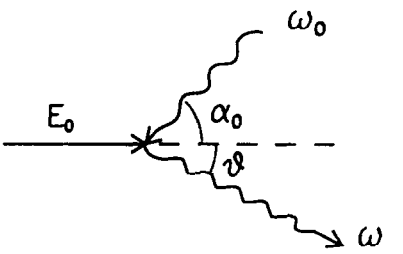

Fig. 1. Kinematics of Compton scattering.

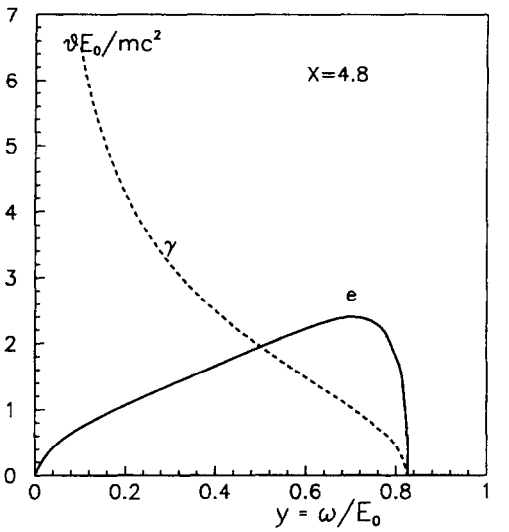

Fig. 2. Electron and photon scattering angles vs. photon energy for $x = 4.8$.

The photon and electron scattering angles are unique functions of the photon energy:

$$\vartheta_\gamma(y) = \vartheta_0\sqrt{\frac{y_m}{y} - 1}, \qquad \vartheta_e = \vartheta_\gamma\frac{y}{1-y}, \tag{2}$$

where $y = \omega/E_0$. These functions for $x = 4.8$ are displayed in Fig. 2.

Table 1
Some parameters of 0.5 TeV linear colliders

	VLEPP (Russia)	NLC (SLAC)	JLC(X) (KEK)	CLIC (CERN)	DLC (DESY)	TESLA (DESY)
L, 10^{33} cm^{-2}s^{-1}	12	8	6.3	2.2–8.9	3.7	6.5
Rep. rate, Hz	300	180	150	1700	50	10
# bunch/train	1	90	90	1–4	125	800
Part./bunch (10^{10})	20	0.65	0.63	0.6	2.9	5.2
σ_x (nm)	2000	300	260	90	670	1000
σ_y (nm)	4	3	3	8	30	65
σ_z (mm)	0.75	0.1	0.07	0.17	0.5	1
Δt bunch (ns)	–	1.4	1.4	0.33	16	1000

The energy spectrum of the scattered photons is defined by the cross section

$$\frac{1}{\sigma_c}\frac{d\sigma_c}{dy} \equiv f(x, y) = \frac{2\sigma_0}{x\sigma_c}\left[\frac{1}{1-y} + 1 - y - 4r(1-r) + 2\lambda_e P_c r x(1-2r)(2-y)\right]; \quad (3)$$

$$y = \frac{\omega}{E_0} \le y_m = \frac{x}{x+1};$$

$$r = \frac{y}{x(1-y)} \le 1;$$

$$\sigma_0 = \pi\left(\frac{e^2}{mc^2}\right)^2 = 2.5 \times 10^{-25}\ \text{cm}^2.$$

The electron mean helicity is $\lambda_e (|\lambda_e| \le \frac{1}{2})$, and that of the laser photons is P_c.

The total Compton cross section is

$$\sigma_c = \sigma_c^{np} + 2\lambda_e P_c \sigma_1, \quad (4)$$

$$\sigma_c^{np} = \frac{2\sigma_0}{x}\left[\left(1 - \frac{4}{x} - \frac{8}{x^2}\right)\ln(x+1) + \frac{1}{2} + \frac{8}{x} - \frac{1}{2(x+1)^2}\right],$$

$$\sigma_1 = \frac{2\sigma_0}{x}\left[\left(1 + \frac{2}{x}\right)\ln(x+1) - \frac{5}{2} + \frac{1}{x+1} - \frac{1}{2(x+1)^2}\right].$$

In the region of our interest $x = 1$–10 the ratio $|\sigma_1/\sigma_c| < 0.2$, i.e. the total cross section only depends slightly on the polarization. However, the energy spectrum does essentially depend on the value of $2\lambda_e P_c$. At $2\lambda_e P_c = -1$ and $x > 2$ the relative number of hard photons nearly doubles (Fig. 3), improving essentially the monochromaticity of the photon beam.

The photon energy spectrum presented in Fig. 3 corresponds to the case of a small conversion coefficient. In a "thick" target each electron may undergo multiple Compton scatterings. The secondary photons are softer in general and populate the low part of spectrum. In Fig. 4 are plotted the photon spectra for various thicknesses of a laser target expressed in units of the collision length for electrons of the initial energy. In the same picture the ratio of the total number of produced photons to the number of photons produced by primary electrons is also given. Multiple Compton scatterings lead to an increase of $\gamma\gamma$ luminosity at low and intermediate invariant masses (that is positive), but, on the other hand, they spoil the polarization properties of scattered photons (see Section 3.3) and also produce background in the detector ($\gamma\gamma \to$ hadrons, see Section 9).

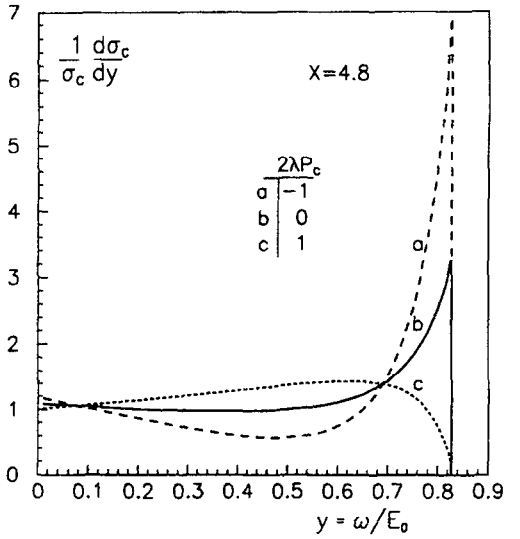

Fig. 3. Energy spectra of scattered photons for different polarizations.

3.2. Choice of a laser wavelength

By increasing the energy of the laser photons, the maximum energy of the scattered photons also increases and monochromaticity of the spectrum improves. However, besides Compton scattering, other processes become possible in the conversion region [3,7]. The most important one is the process of e^+e^- pair creation in the collision of a laser photon with a high energy scattered photon. The threshold of this reaction is $\omega_m \omega_0 > m^2c^4$, i.e.

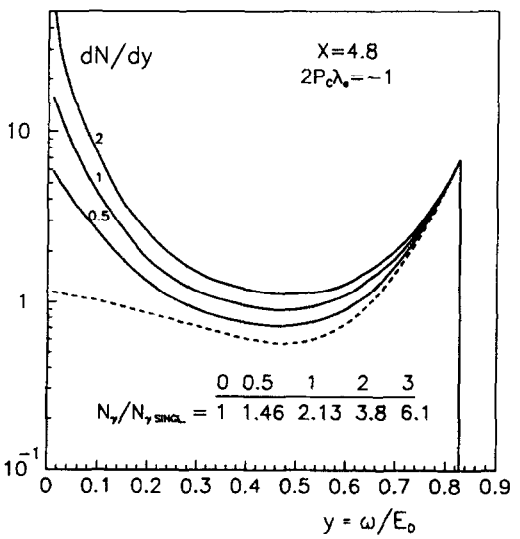

Fig. 4. Normalized (to maximum) photon spectra for different numbers of interaction lengths in a laser target (these numbers mark the solid curves); dashed curve is photon spectra without secondary scatterings.

$x > 2(1+\sqrt{2}) \approx 4.83$. At $x = 4.8$ the wavelength or the energy of the laser photons are the following

$$\lambda = 4.2 E_0[\text{TeV}]\ \mu\text{m}; \quad \omega_0 = 0.3/E_0[\text{TeV}]\ \text{eV}. \tag{5}$$

Above the threshold region ($x \sim 8$–20) the pair production cross section exceeds the Compton one by a factor of 1.5–2 (see Fig. 5 [7], [8]). Due to this fact the maximum conversion coefficient at large x is limited by 25–30%. For these reasons it is preferable to work at $x \sim 4.8$.

3.3. Polarization of photons

If electrons or laser photons are longitudinally polarized, the scattered high energy photons have circular polarization too. The mean photon helicity is given by [6]:

$$\lambda_\gamma(y) = \left[2\lambda_e x r\left[1+(1-y)(1-2r)^2\right] + P_c(1-2r)\left(\frac{1}{1-y}+1-y\right)\right] \Big/ \left[\frac{1}{1-y}+1-y-4r(1-r) + 2P_c\lambda_e r x(1-2r)(2-y)\right], \tag{6}$$

where y and r were defined before. This is shown in Fig. 6 for various helicities of electron and laser beams. Note, if polarization of laser photons $P_c = \pm 1$, then $\lambda_\gamma = -P_c$ at $y = y_m$. In the case of $2P_c\lambda_e = -1$ (the case with good monochromaticity) all the photons in the high energy peak have a high degree like-sign polarization.

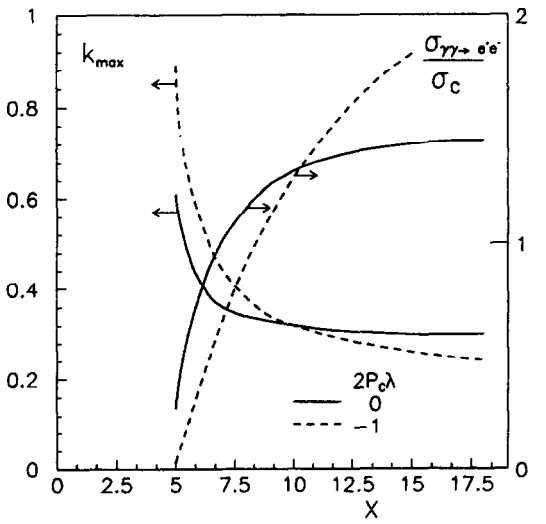

Fig. 5. (a) The ratio of cross sections for e^+e^- pair creation in the collision of laser and high energy photons and for Compton scattering and (b) dependence of the maximum conversion coefficient on x assuming $\omega = \omega_m$.

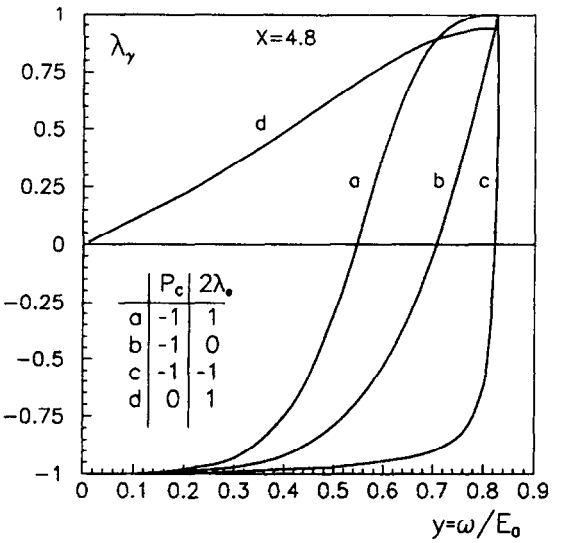

Fig. 6. Helicity of scattered photons vs. ω/E_0 for various polarizations of laser and electron beams.

One can also produce photons with a transverse polarization [6], but it is less useful than longitudital.

Polarization characteristics of the luminosity are discussed in the next session. The polarization is crucial for some experiments [16,10].

3.4. Spectral luminosity, monochromaticity

The spectrum of the scattered photons is very broad, but because of the energy–angle correlation in Compton scattering it is possible to obtain rather narrow distributions of the spectral luminosities of $\gamma\gamma$ and γe collisions. The spectral luminosity distributions depends on the vari-

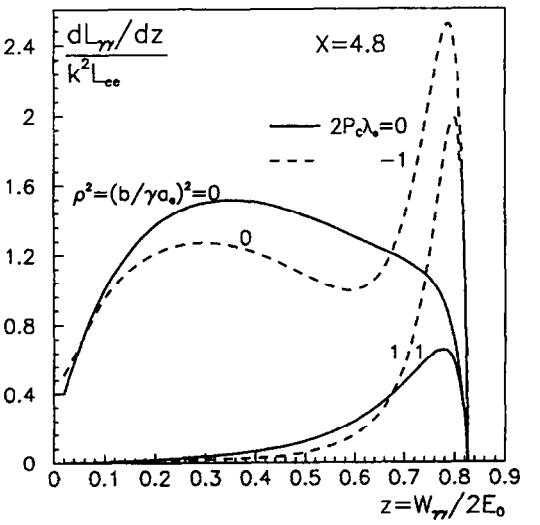

Fig. 7. Spectral luminosity of $\gamma\gamma$ collisions.

able $\rho = b/\gamma a$, where b is the distance between the conversion region and the interaction point (i.p.), and $a \equiv a_e$ is the r.m.s. radius of the electron beam at the i.p. If $\rho \ll 1$, then at the i.p. photons of various energies are mixed in space and the distribution in the invariant mass of the $\gamma\gamma$ of γe system is broad. But, if $\rho \gg 1$, then in γe collisions electrons collide only with the highest energy photons, therefore the invariant mass spectrum of a γe collision is narrow. In $\gamma\gamma$ collisions at $\rho \gg 1$ the photons with higher energy collide at a smaller spot size and, therefore, contribute more to the luminosity. As a result, the luminosity spectrum is much narrower than at $\rho \ll 1$.

For round beams the distribution of luminosity in invariant mass of $\gamma\gamma$ system $W_{\gamma\gamma}$ has the form [3]

$$\frac{dL_{\gamma\gamma}}{dz} = 2zk^2L_{ee}\int_{z^2/y_m}^{y_m} f(x, y)f(x, z^2/y) \times I_0(\rho^2(x+1))\sqrt{\left(\frac{y_m}{y}-1\right)\left(\frac{y_m y}{z^2}-1\right)} \times \exp\left[-\left(\frac{y_m}{y}+\frac{y_m y}{z^2}-2\right)\frac{(x+1)\rho^2}{2}\right]\frac{dy}{y}, \quad (7)$$

where $z = W_{\gamma\gamma}/2E_0$, $\rho = b/\gamma a$, $f(x, y)$ is defined in Eq. (3), $I_0(x)$ is the Bessel function for an imaginary argument and $L_{ee} = N^2 f/2\pi a^2$. In Fig. 7 the plots of spectral luminosities are shown for unpolarized and polarized beams ($2P_c\lambda_e = -1$ both beams) for $\rho = 0$ and 1. One can see that at $\rho = 1$ the luminosity in the low mass region is strongly suppressed and the full width at half of maximum is about 10% for polarized and 20% for unpolarized beams.

Figures for the dependence of the monochromaticity and $\gamma\gamma$ luminosity on ρ^2 can be found in Ref. [7].

Let us consider here the ultimate case: $\rho \gg 1$. In this case the spectral $\gamma\gamma$ luminosity is given by the simple formula [3]

$$\frac{dL_{\gamma\gamma}}{dz} = \frac{k^2N^2\gamma^2}{\pi x b^2} z^2 f^2(x, z). \quad (8)$$

The monochromaticity of collisions can be characterized by the value of

$$A = \frac{1}{L_{\gamma\gamma}}\frac{dL_{\gamma\gamma}}{dz}z_{max} \quad \text{at} \quad z = z_{max}. \quad (9)$$

The reverse value $\eta = 1/A$ is approximately equal to the relative full width of the luminosity distribution at half maximum. The value of A is plotted in Fig. 8a as a function of x. One can see that at $x = 5$ the width of spectrum $1/A \sim 5\%$ for polarized beams and 10% for unpolarized beams and it improves with increasing x. In the case of polarized beams at $x = 20$ the monochromaticity is already 1.5%! Although at $x = 20$ the maximum conversion coefficient is only about 20% (Section 3.2), and the luminosity is by one order of magnitude lower then at $x \lesssim 4.8$, nevertheless in some experiments the ultimate monochromaticity will be very useful. For example, the search for narrow resonances at large nonresonant background (Higgs, for example) requires $\int Ldt \propto 1/A$ and for resonance study $\int Ldt \propto 1/A^2$.

According to Fig. 8a the monochromaticity for polarized ($2P_c\lambda_e = -1$) beams is by a factor 2 higher than for the unpolarized case. The difference is considerably higher when we compare *absolute* peak luminosities ($dL_{\gamma\gamma}/dz$ at $z = z_{max}$) at the same distance b between conversion and interaction regions (see Fig. 8b). The ratio of peak differential luminosities is 4.4 and 7.4 for $x = 5$ and $x = 20$ respectively. The total luminosity/beam collision at $\rho \gg 1$ is

$$L_{\gamma\gamma} = \frac{N^2k^2\gamma^2}{4\pi b^2}F(x), \quad (10)$$

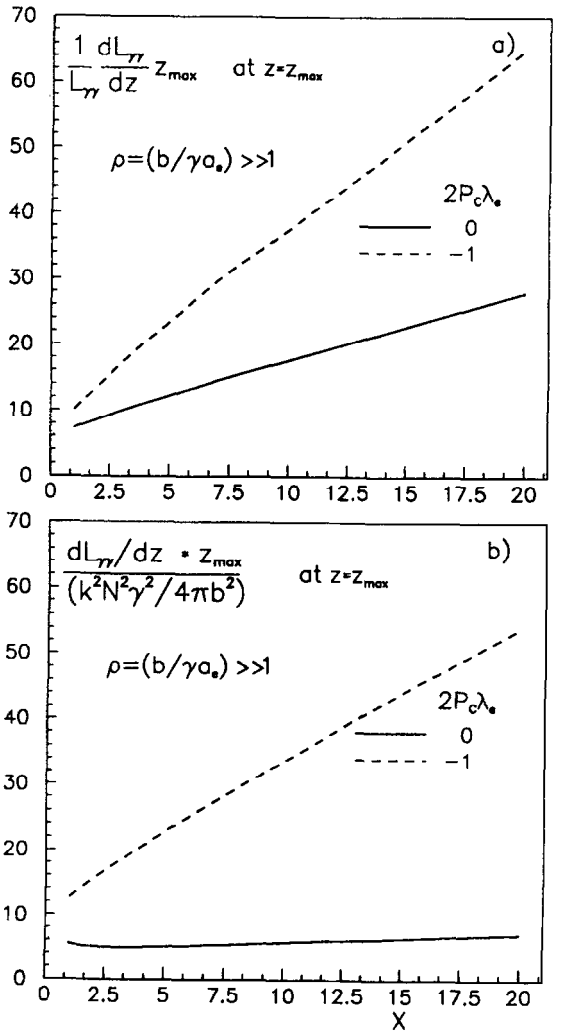

Fig. 8. Peak differential $\gamma\gamma$ luminosity at $\rho^2 = (b/\gamma a_e)^2 \gg 1$ vs. x: (a) normalized peak luminosity, (b) absolute peak luminosity for a fixed distance b between interaction and conversion regions.

where, with 15% accuracy,

$F(x) = 0.72 - 0.16 \ln x$ for unpolarized beams,

$F(x) = 1.25 - 0.16 \ln x$ for $2P_c\lambda = -1$.

At $x = 4.8$ for these two cases $F = 0.42$ and 1 respectively.

The last remark about the case $\rho \gg 1$ is that one may think that an increase of ρ leads inevitably to a decrease of the $L_{\gamma\gamma}$ luminosity. It is correct when we increase the distance between the conversion and the interaction region, in this case $L_{\gamma\gamma} \propto 1/\rho^2$. But one can do the same by decreasing the electron beam radius, in this case $L_{\gamma\gamma} \to$ const. as $\rho \to \infty$.

The possible helicities of two colliding photons is 0 or 2, so $dL_{\gamma\gamma}/dz$ can be decomposed in two parts: dL_0/dz and dL_2/dz [6,34]. These luminosities are plotted in Figs. 9a–9c for $x = 4.8$, $P_c = 1$ and $2\lambda_e = -1$, -0.5, 0 (equal for both beams). The ratio L_0/L_2 for the region $0.75 \le z \le z_{max}$ vs λ_e is shown in Fig. 9d. For 100% electron polarization $L_0/L_2 \sim 60$ (by changing the polarization of one laser and the corresponding electron beam to the opposite, one can get the reverse case). This is of great importance for Higgs measurements, because $N_{\gamma\gamma \to H} \propto 1 + \lambda_{\gamma 1}\lambda_{\gamma 2} \propto L_0$, while for main background $N_{\gamma\gamma \to \bar{q}q} \propto 1 - \lambda_{\gamma 1}\lambda_{\gamma 2} \propto L_2$ [16,10].

We have seen that for $2P_c\lambda_e \sim -1$ the ratio L_0/L_2 is large in the high energy peak. In this case one can work at $\rho \gg 1$ with a good monochromaticity. For the opposite cases $2P_c\lambda_e \sim +1$, the ratio L_0/L_2 is large in a wide range of invariant masses (see Fig. 10), so, at first sight, it is convenient for the purpose of searching for the Higgs [10]. But in this case, in order to have a broad spectrum, one has to work at $\rho \ll 1$. However, in this regime the $\gamma\gamma$ luminosity may be much lower than at $\rho \gg 1$ (if b is fixed and one artificially increases the electron cross section). Another important note is that the luminosity in the intermediate invariant region is greatly populated by collisions of photons produced in the secondary Compton scatterings; this considerably deteriorates the polarization. At last, as was pointed out by Richard [17] at this Workshop, there is a very large background for Higgs due to the process $\gamma g \to b\bar{b}$. Gluons in a photon carry in general a small part of the photon energy, and only operation with good monochromaticity, at $z \sim z_{max}$, can eliminate this background.

For γe collisions the formulae for luminosities can be found elsewhere [3]. Note only that with an increase of ρ

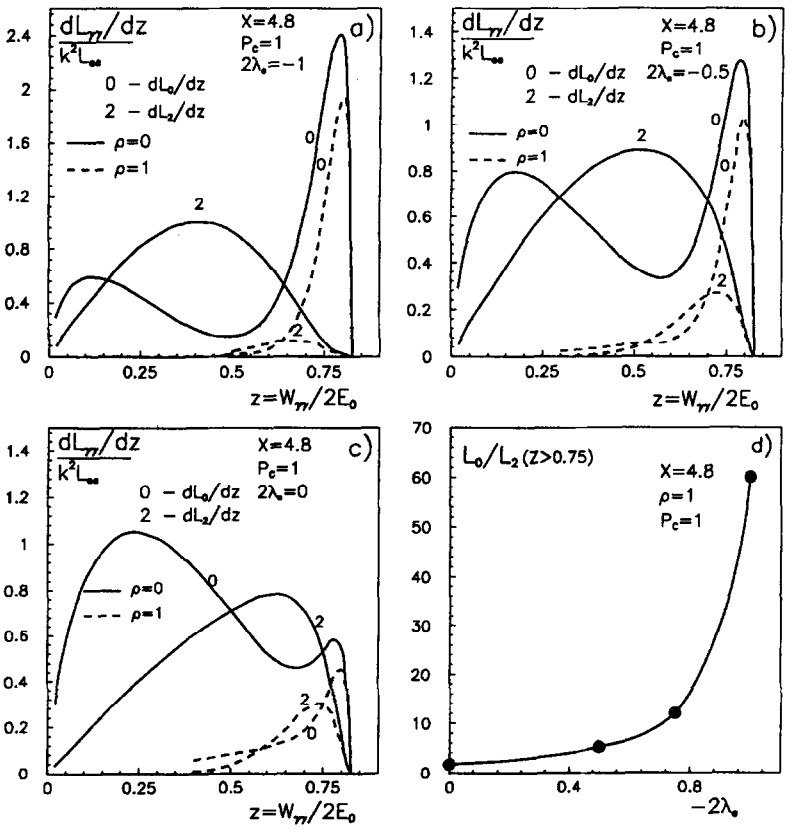

Fig. 9. (a–c) Spectral luminosities L_0 and L_2 for various degrees of electron polarization λ_e in the case of a laser helicity $P_c = 1$ and $\lambda_e < 0$; (d) ratio L_0/L_2 at $z > 0.75$ vs. degree of the electron polarization.

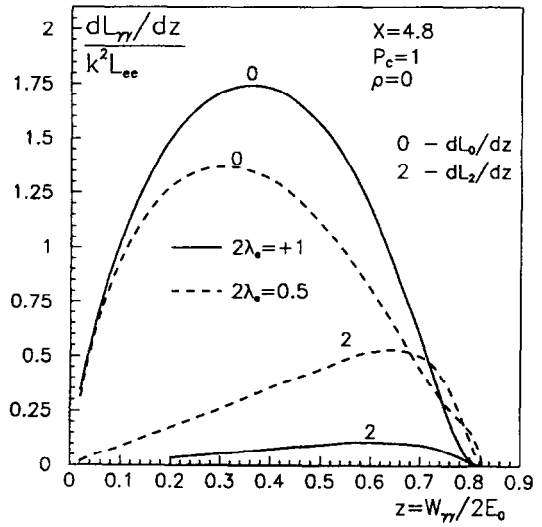

Fig. 10. Spectral luminosities L_0 and L_2 for the case $P_c = 1$ and $\lambda > 0$.

the monochromaticity of γe collisions improves up to monochromaticity of electron beams (for any values of x).

In this section we have considered only kinematical characteristics of the luminosities. The collision effects, which determine attainable luminosity, are considered in Section 5.

4. Conversion coefficient, requirement of lasers

4.1. Estimation of the conversion coefficient

The conversion coefficient depends on the energy of the laser flash A as

$$k = N_\gamma/N_e \sim 1 - \exp(A/A_0) \quad (\sim A/A_0 \text{ at } A < A_0). \tag{11}$$

Let us estimate A_0. At the conversion region the r.m.s. radius of the laser beam depends on the distance z to the focus (along the beam) in the following way [3]:

$$r_\gamma = a_\gamma\sqrt{1 + z^2/\beta_\gamma^2}, \tag{12}$$

where $\beta_\gamma = 2\pi a_\gamma^2/\lambda$, a_γ is the r.m.s. focal spot radius, and λ is the laser wavelength. The expression for β_γ is valid for a Gaussian shape of the beam in the diffraction limit of focusing. The density of laser photons

$$n_\gamma = \frac{A}{\pi r_\gamma^2 \omega_0}\exp\left(-r^2/r_\gamma^2\right)F_\gamma(z + ct),$$

$$\int F_\gamma(z)\,dz = 1. \tag{13}$$

Let us assume that the linear photon density is uniform along the beam: $F_\gamma = 1/l_\gamma$ and $\beta_\gamma \ll l_\gamma$. The probability of Compton scattering for the electron moving through a laser target along the axis

$$p = 2\int n_\gamma \sigma_c\,dz \sim \frac{2A\sigma_c}{\pi a_\gamma^2 l_\gamma}\int_{-\infty}^{\infty}\frac{dz}{1 + \dfrac{z^2}{\beta_\gamma^2}} = \frac{2A\sigma_c}{c\hbar l_\gamma}. \tag{14}$$

The factor 2 in the first equality is due to the relative motion of electrons and photons. The effective interaction length is given by the intergal and equals $\pi\beta_\gamma$. The probability $p = 1$ ($A = A_0$) at

$$A_0 = \frac{\hbar c l_\gamma}{2\sigma_c} \quad \text{and} \quad P = \frac{A_0 c}{l_\gamma} = \frac{\hbar c^2}{2\sigma_c}. \tag{15}$$

To provide the high photon density at the laser focus during the collision with the electron bunch of length l_e, the laser bunch should have the length $l_\gamma > l_e$. The minimum laser flash energy and laser power needed for obtaining the conversion coefficient $k \sim 65\%$ ($A = A_0$ in Eq. (11)) at $x = 4.8$ ($\sigma_c \approx 9 \times 10^{-25}\text{cm}^2$) are

$$A_{0,\min} = \frac{\hbar c l_e}{2\sigma_c} = 8.4 l_e[\text{cm}]\ \text{J}, \tag{16}$$

$$P_{0,\min} = \frac{A_0 c}{l_\gamma} = \frac{\hbar c^2}{2\sigma_c} \approx 2.5 \times 10^{11}\ \text{W}. \tag{17}$$

These minimum values for A_0 and P_0 have been obtained for a uniform photon density distribution along electron and laser beams and $\beta_\gamma \ll l_e = l_\gamma$. For Gaussian beams with $l_e = l_\gamma \equiv 2\sigma_z \gg \beta_\gamma$,

$$A_0 \approx \sqrt{\pi}\,A_{0,\min} \quad \text{and} \quad P_{\text{peak}} \approx \sqrt{2}\,P_{0,\min}. \tag{18}$$

It is remarkable that the value of A_0 is almost independent of the focal spot size until $2\beta_\gamma < l_e = l_\gamma$, i.e. $a_\gamma < \sqrt{\lambda l_e/4\pi}$. When the focal radius a_γ is decreased, then the length of the region with high photon density becomes shorter and the probability of conversion almost does not change.

Let us consider another example: $2\beta_\gamma \approx l_\gamma \geq l_e$. In this case A_0 is only slightly larger than $A_{0,\min}$, but the laser target has a relatively low density (and large length (β_γ)) that is important to avoid multiphoton processes to be discussed in the next section. In this case the radius of laser beam $r_\gamma \sim a_\gamma$ along the target and the density of laser photons $n_\gamma \sim A/(\pi\omega_0 a_\gamma^2 l_\gamma)$. The probability of conversion $p \sim n_\gamma \sigma_c l_\gamma = 1$ at

$$A_0 = \frac{\pi\hbar c l_\gamma}{2\sigma_c} = \pi A_{0,\min} = 25 l_\gamma[\text{cm}]\ \text{J}. \tag{19}$$

Here, as before, we assumed $x = 4.8$. With such a focusing the angular divergence of the laser light is

$$\alpha_\gamma = a_\gamma/\beta_\gamma = \lambda/2\pi a_\gamma \approx \sqrt{\lambda/\pi l_e}. \tag{20}$$

The value of A_0 only slightly varies until the collision angle $\alpha_0 < \alpha_\gamma$. For $\alpha_0 \gg \alpha_\gamma$, A_0 is larger by a factor χ

$= \sqrt{\pi}\,\alpha_0/\alpha_\gamma$ [3], although, in principle, using complicated optics one can get the same A_0 for any collision angle.

4.2. Influence of a strong field on processes in the conversion region

In the conversion region the density of laser photons can be very high, which leads to multiphoton processes [18,19]:

$$e + n\gamma \to e + n\gamma_0, \quad \gamma + n\gamma_0 \to e^+e^-,$$

where e, γ are a high energy electron and photon respectively, and γ_0 denotes a laser photon. Nonlinear effects are described (partially) by the parameter

$$\xi = \frac{eF\hbar}{m\omega_0 c}, \tag{21}$$

where F is the field strength (E,B) and ω_0 is the photon energy. At $\xi \ll 1$ an electron interacts with one photon from the field (Compton scattering), while at $\xi \gg 1$ an electron feels a collective field (synchrotron radiation).

What values of ξ are acceptable? In a strong field electrons have a transverse motion, which increases the effective mass of the electrons [18]: $m^2 \to m^2(1+\xi^2)$. Due to this fact at $\xi^2 = 0.3$ (and $x = 4.8$) y_m decreases by 5%.

What is the value of ξ in the our case? Assuming $2\beta_\gamma \approx l_\gamma$ (the case of a low density target, see previous subsection) and taking into account that the field in the laser focus is $F^2 = 4A/a_\gamma^2 l_\gamma$ and $A = kA_0$ (Eq. (19)) one gets [7,8]

$$\xi^2 \approx \frac{2}{\pi\alpha}\frac{\sigma_0}{\sigma_c}\frac{\lambda}{l_\gamma}k. \tag{22}$$

At $x = 4.8(\sigma_c/\sigma_0 = 0.75$ and $\lambda = 4.2E_0(\text{TeV})$ μm) and $k = 1$ we get

$$\xi^2 = 0.05E_0[\text{TeV}]/l_\gamma. \tag{23}$$

For example, if $l_\gamma = l_e = 200$ μm and $E_0 = 1$ TeV, then $\xi^2 = 2.5$. This is not acceptable. To decrease ξ, keeping $k = \text{const}$, one has to use a longer photon bunch, i.e. l_γ must be longer than l_e. From Eq. (23) it follows that, if $\xi^2 = 0.3$, then

$$l_\gamma \approx 0.17E_0[\text{TeV}]\ \text{cm}. \tag{24}$$

Substituting l_γ instead of l_e into Eq. (19) we get

$$A_0 \approx 4E_0[\text{TeV}]\ \text{J}. \tag{25}$$

For large E_0 and short bunches this requirement to the energy A_0 is stronger, than follows from the simple consideration of the conversion probability, Eqs. (16) and (18).

4.3. Lasers

From two previous sections follows that to obtain the conversion probability $k = 65\%$ $(A = A_0)$ at $x = 4.8$ a laser with the following parameters is requried:

Flash energy:	$A_0 \sim \max(15l_e\ [\text{cm}], 4E_0\ [\text{TeV}], \text{J};$
Duration:	$ct = \max(l_e, 0.17\ E\ [\text{TeV}]), \text{cm};$
Repetition rate:	n bunches × rep.rate of a collider;
Wavelength:	$\lambda = 4.2\ E_0\ [\text{TeV}]$ μm or $\omega_0 = 0.3/E_0\ [\text{TeV}]$ eV;
Angular divergence:	near the diffraction limit.

The first numbers for flash energy and duration are determined by diffraction, the second by nonlinear effects in the conversion region. For example, at $E_0 = 0.25$ TeV and $l_e = 200$ μm (SLAC, KEK) a laser with a flash energy $A \sim 1$ J, $l_\gamma \sim 400$ μm and $\lambda = 1$ μm is required. The first two numbers are determined by nonlinear effects. For TESLA with $l_e = 2$ mm a laser with $A \sim 3$ J and $l_\gamma \sim 0.2$ mm is required. Here, nonlinear effects are not essential.

Obtaining Joule pulses of picosecond duration is not a problem for modern laser technique. The main problem is a high repetition rate. Nice reviews on achievements and perspectives of conventional lasers for photon colliders were given by Geissler [20] and Meyerhofer [21]. Solid state lasers with a few joule flash energy and picosecond duration have a repetition rate of only about a few Hz. This is connected with overheating of the media. For example, a Nd:glass laser ($\lambda = 1.06$ μm used now in experiment E-144 at SLAC [21] has 2 TW power and 1 ps duration. It is exactly what is needed for the collider with $2E_0 = 500$ GeV energy. However, its repetition rate is only 1 Hz. Replacing pumping flashlamps by diodes (lasers) will substantially reduce the thermal problem and the repetition rate can be increased up to 100 Hz [21]. An array of 10–100 slabs will provide a repetition rate sufficient for photon colliders. Gas lasers have also good parameters and perspectives.

The success in obtaining picosecond pulses is connected with a chirped pulse technique ("chirped" means time–frequency correlation in the pulse). After amplification a long chirped pulse is compressed using a grating

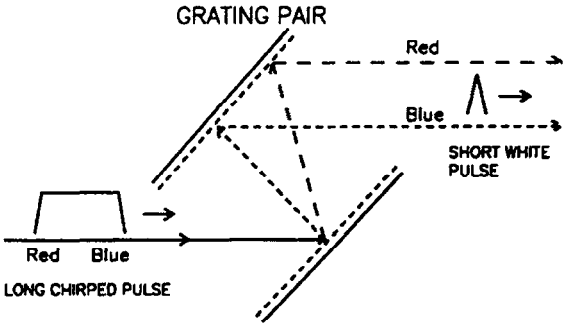

Fig. 11. Compression of a chirped laser pulse using grating pair.

pair to picosecond duration (see Fig. 11). Stretching and compression by a factor of 1000 has been demonstrated.

Very attractive lasers for photon linear colliders are free-electron lasers [5]. They have a tunable wavelength and a high repetition rate. However, it will be difficult to generate joules in 1 ps. The task becomes much simpler, if the FEL generates a long chirped pulse, which is compressed after that by a grating pair [8].

Analyses carried out by FEL experts [22–25] show that there are no (very) serious problems in the way of FEL for photon colliders (except money) and they should be developed right now together with linear colliders.

5. Collision effects, ultimate luminosities of $\gamma\gamma$, γe collisions

5.1. Collision schemes

It is well known that for e^+e^- linear colliders collision effects (beamstrahlung and beam instability) impose strict restrictions on beam parameters and determine the attainable luminosity. At first sight in γe and $\gamma\gamma$ collisions at least one of the beams is neutral so that collision effects are absent. This is not the case. Let us first consider how beams are colliding. Three schemes are discussed:

Scheme A: The conversion region is situated close to the interaction point (i.p) at a distance $b \sim 2\sigma_z$, and after conversion all particles travel directly to the i.p. [8,26].

Scheme B: After conversion at some distance b from the interaction region the particles pass the region with the transverse magnetic field, where "used" electrons are swept aside in the horizontal (x) (or vertical (y)) direction by a distance larger than σ_x [3,7,8]. Thereby one gets more or less clean γe or $\gamma\gamma$ collisions.

Scheme C: After conversion electrons are defocussed by a plasma lens. This idea was proposed at this workshop [27]. Here I will not consider this interesting approach.

The first scheme is simple, but background conditions are much worse (mixture of $\gamma\gamma$,γe,ee collisions, larger disruption angles), although, for $\gamma\gamma$ collisions at a proper choice of beam parameters, the γe,ee background is substantially suppressed owing to beams repulsion. Below we will consider both schemes A and B and compare attainable luminosities.

5.2. Beam collision effects

During beam collisions electrons and photons are influenced by the field of the opposing electron beam. In the case of $\gamma\gamma$ collisions the field is created by "used" electrons deflected after conversion by the external field (not deflected in the scheme A). In γe collisions the field is also created by the main electron bunch used for γe collisions. A strong field leads to:

- energy spread of the electrons in γe collisions;
- conversion of photons into e^+e^- pairs in γe and $\gamma\gamma$ collisions (coherent pair creation);
- beam displacement in γe collisions.

These effects determine attainable $\gamma\gamma$, γe luminosities. Let us consider them.

5.2.1. Coherent pair creation in the beam field

The probability of pair creation per unit length by a photon with energy ω in a magnetic field B ($|B|+|E|$ for our case) is [7,8,28,29]

$$\mu(\kappa) = \frac{\alpha^2}{r_e}\frac{B}{B_0}T(\kappa), \tag{26}$$

where

$$\kappa = \frac{\omega}{mc^2}\frac{B}{B_0},$$

$$B_0 = \frac{m^2c^3}{e\hbar} = 4.4\times 10^{13}\ \mathrm{G}$$

is the the critical field, and $r_e = e^2/mc^2$ is the classical radius of the electron.

$$\begin{aligned} T(\kappa) &\approx 0.16\kappa^{-1}K^2_{1/3}(4/3\kappa), \\ &\approx 0.23\exp(-8/3\kappa) \quad \text{for} \quad \kappa \ll 1, \\ &\approx 0.38\kappa^{-1/3} \quad \text{for} \quad \kappa \gg 1. \end{aligned} \tag{27}$$

In our case $\omega \sim E_0$; therefore one can put

$$\kappa \sim \Upsilon \equiv \gamma B/B_0. \tag{28}$$

The probability to create e^+e^- pair during the collision time is

$$p \approx \mu\sigma_z = \frac{\alpha^2\sigma_z}{r_e\gamma}\Upsilon T(\Upsilon). \tag{29}$$

If we allow some pair creation probability p, then from this equation one can find the corresponding Υ. In Table 2 the values of Υ_p are presented for $p = 0.05$ and various σ_z and E_0. We provided Υ with the index p to designate effect of "pair creation". One can see that for existing projects $\Upsilon_p \sim 1$.

5.2.2. Radiation energy losses of electrons (beamstrahlung) in γe collisions

The field of the opposing beam leads to beamstrahlung. The relative energy loss of an electron in field B per

Table 2
Values of Υ_p for p = 0.05

σ_z, cm	E_0, TeV		
	0.25	0.5	1.0
0.01	1.32	1.43	1.67
0.05	0.74	0.9	1.2
0.1	0.62	0.74	0.91

Table 3
Values of T_b for $\delta = 0.05$

σ_z, cm	E_0, TeV		
	0.25	0.5	1.0
0.01	0.19	0.33	0.52
0.05	0.07	0.11	1.16
0.1	0.048	0.07	0.11

collision length $\sim \sigma_z$ is [7,8,30,31]

$$\delta = \frac{\Delta E}{E_0} \sim \frac{2\alpha^2}{3r_e\gamma} T^2 \; F(T)\sigma_z, \tag{30}$$

where T was defined above and

$$F(T) \approx 1/(5T+1) \quad \text{for} \quad T < 100. \tag{31}$$

Value of δ is restricted usually to the level 1–10%. For a given δ one can find T_b (index b is "beamstrahlung"). In Table 3 the values of T_b are presented for $\delta = 0.05$ and various σ_z and E_0.

It is of interest that, if δ is small, then the pair creation probability is also small.

5.2.3. Beam–beam displacements

In Scheme A of γe collisions (without deflection) the main electron bunch collides with the opposing "used" electron bunch. Let us assume for simplicity, that all "used" electrons have energies equal to E_0. The problem of instabilities of e^+e^- and e^-e^- beams is well known [32]. If e^-e^- luminosity drops, then $L_{\gamma e}$ will go down as well. The maximum attainable ee luminosity due to this effect

$$L_{ee,max} \approx \frac{\pi N \gamma f}{8 r_e \sigma_z}, \tag{32}$$

where f is the collision rate. $L_{\gamma e}$ is only smaller.

If "used" beam is deflected (Scheme B) after conversion by the distance x_0, then due to repulsion the main bunch is displaced during collision by a distance

$$\Delta x \sim \frac{eB\sigma_z^2}{E_0} \sim \frac{\sigma_z r_e N}{\gamma x_0}. \tag{33}$$

The luminosity is not lost if $\Delta x < \sigma_x$, so when

$$x_0 > \frac{\sigma_z r_e N}{\gamma \sigma_x}. \tag{34}$$

5.2.4. Beam fields, deflection

The field produced at the i.p. by "deflected" (by an external field) electrons of the converted beam is approximately equal to [8]

$$B_d \equiv |E| + |B| \sim \frac{2eN(1-0.5k)}{\sigma_z x_0}, \tag{35}$$

where x_0 is the deflection of electrons with the energy E_0. The field inside the "main" electron beam

$$B_m \sim \frac{eN}{\sigma_x \sigma_z}. \tag{36}$$

From Eq. (36) and connection $T_p = \gamma B/B_0$ we get

$$\sigma_x = \frac{eN}{\sigma_z B_m} = \frac{\gamma eN}{\sigma_z B_0 T_p} = \frac{N r_e^2 \gamma}{\alpha \sigma_z T_p}, \tag{37}$$

where T_p is given in Table 2.

To provide a deflection x_0 in the external field B_e it is necessary to have a distance between the conversion region and the i.p.

$$b^2 = \frac{2E_0 x_0}{eB_e} = \frac{4N\gamma^2 e r_e (1-0.5k)}{\alpha B_e \sigma_z T_b}, \tag{38}$$

where T_b is given in Table 3.

5.3. Ultimate luminosity in γe collisions

5.3.1. Scheme A (without deflection)

There are three collision effects here: beamstrahlung; pair creation; and beam–beam instabilities.

As was pointed out in the previous section, if beamstrahlung losses are small, then the pair creation probability is also small: $p < \delta \ll 1$. The other two points are the same as for ee collisions. Therefore

$$L_{\gamma e,max} \sim kL_{ee}. \tag{39}$$

5.3.2. Scheme B (with deflection)

The maximum γe luminosity is

$$L_{\gamma e} \sim \frac{kN^2 f}{4\pi (b/\gamma)\sigma_x}. \tag{40}$$

Here the horizontal beam size is determined by pair creation while the distance b is determined by two effects: beamstrahlung and beam displacement.

Taking σ_x from Eq. (37) and b from Eq. (38) (beamstrahlung) we get

$$L_1^{\gamma e} \sim \frac{\alpha^2 \sigma_z k f T_p}{4\pi r_e^3 \gamma} \left(\frac{B_e \sigma_z T_b N}{4 r_e B_0 (1-0.5k)} \right)^{1/2}. \tag{41}$$

Table 4
The coefficient C in Eq. (42)

σ_z, (cm)s	E_0, TeV		
	0.25	0.5	1.0
0.01	0.46	0.31	0.23
0.05	1.7	1.3	1.04
0.1	3.4	2.4	1.84

For $k = 0.65$ ($A = A_0$), $B_e = 30$ kG and values of Υ_p, Υ_b from Tables 2 and 3 we get

$$L_1^{\gamma e} = \sqrt{\frac{N}{10^{10}}}\, f[\mathrm{Hz}] \times 10^{30} \times C \ \mathrm{cm}^{-2}\mathrm{s}^{-1}, \tag{42}$$

where values of C are given in Table 4. With $\pm 20\%$ accuracy Eq. (42) is described by

$$L_1^{\gamma e} \sim 2\sqrt{\frac{N}{10^{10}}}\, \frac{\sigma_z[\mathrm{cm}] f[\mathrm{Hz}] \times 10^{31}}{\sqrt{E_0[\mathrm{TeV}]}} \ \mathrm{cm}^{-2}\mathrm{s}^{-1}. \tag{43}$$

This is the ultimate $L_{\gamma e}$ due to pair creation and beamstrahlung. If x_0 (and b) are determined by the beam dispalacement during collision and σ_x, as before, by pair creation, then we get

$$L_2^{\gamma e} \le \frac{Nfk\alpha}{4\pi r_e^2}\sqrt{\frac{\gamma B_e \Upsilon_p}{2B_0}}$$

$$\sim 1.3 \times 10^{30}\left(\frac{N}{10^{10}}\right) E^{1/2}[\mathrm{TeV}] f[\mathrm{Hz}] \ \mathrm{cm}^{-2}\mathrm{s}^{-1}. \tag{44}$$

Here we put $\Upsilon_p = 1$; that is good approximation.

A joint limit on γe luminosity is

$$L_{\gamma e} = \min(L_1, L_2). \tag{45}$$

Beam displacement is essential ($L_2 < L_1$) at

$$\sqrt{\frac{N}{10^{10}}}\, \frac{E[\mathrm{TeV}]}{\sigma_z[\mathrm{cm}]} < 15. \tag{46}$$

For different projects $L_{\gamma e,\max}$ is given in Table 5. We see that $L_{\gamma e}$ is good for $2E_0 = 0.5$ TeV, but there will be problems for higher energes.

Beams in γe collisions should be flat. From Eq. (37) at $\Upsilon_p \sim 0.5$ one gets

$$\sigma_x \approx 4 \times 10^{-7}\left(\frac{N}{10^{10}}\right)\frac{E_0[\mathrm{TeV}]}{\sigma_z[\mathrm{cm}]} \ \mathrm{cm}. \tag{47}$$

For $N = 10^{10}$, $\sigma_z = 0.01$ cm we get $\sigma_x = 10^{-5}$ cm at $2E_0 = 0.5$ TeV that is close to σ_x in e^+e^- collisions.

5.4. Ultimate luminosity in $\gamma\gamma$ collisions

5.4.1. Scheme A (without deflection)

In this scheme the electron beams must be flat. The horizontal size σ_x at the i.p. is determined by the coherent pair creation (Eq. (37)); it is the same as for γe collisions (see one paragraph above). The minimum vertical beam size at the i.p. is

$$\sigma_y \sim b/\gamma \sim 2l_\gamma/\gamma, \tag{48}$$

where l_γ is given in Section 4.3. For electron beams with $\sigma_z = 0.1$–0.75 mm and $E = 0.25$–1 TeV, $b_{\min}$ varies between 0.1 and 0.35 cm and $\sigma_y = 2$–6 nm. These numbers are reasonable (see Table 1).

The $\gamma\gamma$ luminosity in this scheme [8]

$$L_{\gamma\gamma} \sim \frac{N^2k^2f}{4\pi\sigma_x\sigma_y} \sim \frac{Nk^2\alpha\sigma_z\Upsilon_p f}{4\pi r_e^2\gamma\sigma_y}$$

$$\sim \left(\frac{N}{10^{10}}\right)\frac{k^2\Upsilon_p\sigma_z[\mathrm{cm}]f[\mathrm{Hz}]}{\sigma_y[\mathrm{nm}]E_0[\mathrm{TeV}]} 3.7 \times 10^{32} \ \mathrm{cm}^{-2}\mathrm{s}^{-1}. \tag{49}$$

Taking Υ_p from Table 2 and assuming $\sigma_y \sim 5$ nm, $k = 0.65$ we get the estimate for the $\gamma\gamma$ luminosity in scheme B (without beam deflection) (see Table 6).

5.4.2. Scheme B (with deflection)

The deflection x_0 and the distance b are determined by pair creation (see Eqs. (35) and (38)). The minimum vertical size of the photon beam at the i.p is $a_\gamma = b/\gamma$; therefore the maximum $\gamma\gamma$ luminosity [7, 8]

$$L_{\gamma\gamma} \sim \frac{N^2k^2f}{4\pi(b/\gamma)^2} = \frac{Nk^2\sigma_z B_e \Upsilon_p f}{16\pi r_e^3 B_0(1-0.5k)}, \tag{50}$$

where $\Upsilon_p \sim 1$ (see Table 2). For $k = 0.65$ ($A = A_0$) and $B = 30$ kG

$$L_{\gamma\gamma} \sim 2\left(\frac{N}{10^{10}}\right) f[\mathrm{Hz}]\sigma_z[\mathrm{cm}]\Upsilon_p \times 10^{32} \ \mathrm{cm}^{-2}\mathrm{s}^{-1}. \tag{51}$$

The results for $E_0 = 0.25$ TeV are presented in Table 7. In this table the $\gamma\gamma$ luminosity per one collision, the photon spot size at the i.p., the distance between the i.p. and the conversion region and the deflection of the con-

Table 5
Ultimate $L_{\gamma e}$, 10^{34} cm^{-2}s^{-1}

$2E_0$, TeV	NLC	DLC	VLEPP	TESLA
0.5	0.6	0.9	0.3	2.0
2	0.3	1	0.2	3.0

Table 6
Ultimate $L_{\gamma\gamma}$, 10^{34} cm^{-2}s^{-1} at $2E_0 = 500$ GeV in Scheme A (without deflection)

NLC	DLC	VLEPP	TESLA
1.5	7.5	3.5	30

Table 7
Ultimate $L_{\gamma\gamma}$, 10^{34} cm^{-2}s^{-1} at $2E_0 = 500$ GeV in Scheme B (with deflection)

	$L_{\gamma\gamma}$, 10^{34}	$L_{\gamma\gamma}$/coll., 10^{30}	a_γ, nm	b, cm	x_0, nm
NLC	3	1.9	10	0.5	40
DLC	12	14	9	0.5	40
VLEPP	6	200	25	1.3	300
TESLA	50	60	12	0.6	60

verted beam (for $E = E_0$) are also given. In this estimation we assumed that the electron beam size at the i.p. is smaller than $a_\gamma \sim b/\gamma$, which is about 10–20 nm (see Table 7). This size is comparable or even larger than σ_y for designed e^+e^- colliders (Table 1), but much smaller than σ_x. Damping rings used usually as injectors produce naturally flat beams and there is a problem in obtaining beam sizes small in both directions.

Comparing Tables 6 and 7 we see that in both schemes with and without deflection the ultimate luminosities are comparable. Each scheme has its advantages and disadvantages.

There is a third intermediate scheme of collisions. As soon as electron beams are naturally flat, then to avoid coherent pair creation one can set Υ_p, by varing σ_x, and make a small separation in the vertical direction to reduce the background of ee and γe collisions. This case is close to Scheme A, but beam repulsion occurs by an external field. At $b = 0.5$ cm the magnetic field of 10 kG separates 250 GeV electron bunches by a distance of 30 nm. Residual ee collisions are no problem; due to beam repulsion ee luminosity will be almost negligible at any reasonable beam parameters. This separation is necessary only for suppression of the residual γe luminosity.

5.5. Disruption angles

After conversion the electrons have a wide energy spectrum. Estimations [7] and simulation (next section) show that at $k = 0.65$ some electrons have an energy as low as 2% of the initial energy. During a beam collision these electrons get kick angles in the field of the opposing beam. In the head-on collision of flat beams soft electrons acquire the angles [7]

$$\vartheta_d \sim \left(\frac{4\pi r_e N}{\sigma_z \gamma_{min}}\right)^{1/2}. \tag{52}$$

For $E_{min} = 0.02E_0$,

$$\vartheta_d \sim 3\left(\frac{N/10^{10}}{\sigma_z[\text{mm}]E_0[\text{TeV}]}\right)^{1/2} \text{mrad}. \tag{53}$$

For NLC, TESLA, DLC at $2E_0 = 500$ GeV, $\vartheta_d \sim 15$ mrad, while for the 100 GeV photon collider considered in Ref. [26]: $E_0 = 100$ GeV, $N = 4 \times 10^{11}$, $\sigma_z = 0.75$ mm, the disruption angle $\vartheta_d \sim 70$ mrad. This estimation describes Scheme A (without deflection) and the "intermediate" scheme (with a small vertical deflection).

In Scheme B with a "large" horizontal deflection (to obtain $\Upsilon_p \sim 1$) particles with smaller energy come to the i.p. with a larger displacement and therefore get a kick in the field of opposing beam which is much smaller than in a head-on collisions.

The results of MC simulation of beam collisions in different schemes are presented in the next section.

6. MC simulation of γγ, γe collisions

As we have seen, the picture of collision is so complicated that the best way to see a final result is the simulation. This program, written by the author only a month ago, takes into account the following processes:

1) Multiple Compton scattering in the conversion region. It was assumed (as a first approximation) that polar-

Table 8
Parameters of beams and results of simulation; the notation a,b · · · f correspond to (a), (b) · · · (f) in Figs. 12 and 13; the two right columns correspond to Fig. 13

	a	b	c	d	e	f	a	b
Type of collisions	γγ	γγ	γγ	γγ	γγ	γγ	γe	γe
# conversion lengths	1, 1	1, 1	1, 1	1, 1	1, 1	1, 1	1, 0	1, 0
$2E_0$, GeV	500	500	500	500	500	200	500	500
$N/10^{10}$	5	5	5	5	5	40	5	1
σ_x, nm	20	6.1	150	150	150	200	50	100
σ_y, nm	20	6.1	20	5	5	4	12	12
σ_z, mm	1	1	1	1	1	0.75	1	0.1
b, cm	1	1	2	0.35	0.35	0.1	3	2
B_x, kG	0	0	0	0	20	0	0	0
B_y, kG	30	30	30	0	0	0	30	30
L(geom), 10^{30}	48	530	6.5	27	27	1600	22	0.65
$L_{\gamma\gamma}$, 10^{30}	10	18	1.7	13	9	750	2.7	0.07
$L_{\gamma\gamma}$ ($z > 0.6$)	5.2	12.8	0.63	2.8	3	165	< 0.003	~ 0
$L_{\gamma e}$, 10^{30}	0.1	0.07	0.017	4.8	0.7	60	3.4	0.28
$L_{\gamma e}$ ($z > 0.6$)	~ 0	~ 0	~ 0	1.6	0.33	13	2.7	0.21
$\vartheta_{x,\,max}$, mrad	4.5	4.2	4.2	6	3	55	4.5	2.5
$\vartheta_{y,\,max}$, mrad	< 0.5	< 0.5	< 0.5	7.5	6.6	42	6	3.6

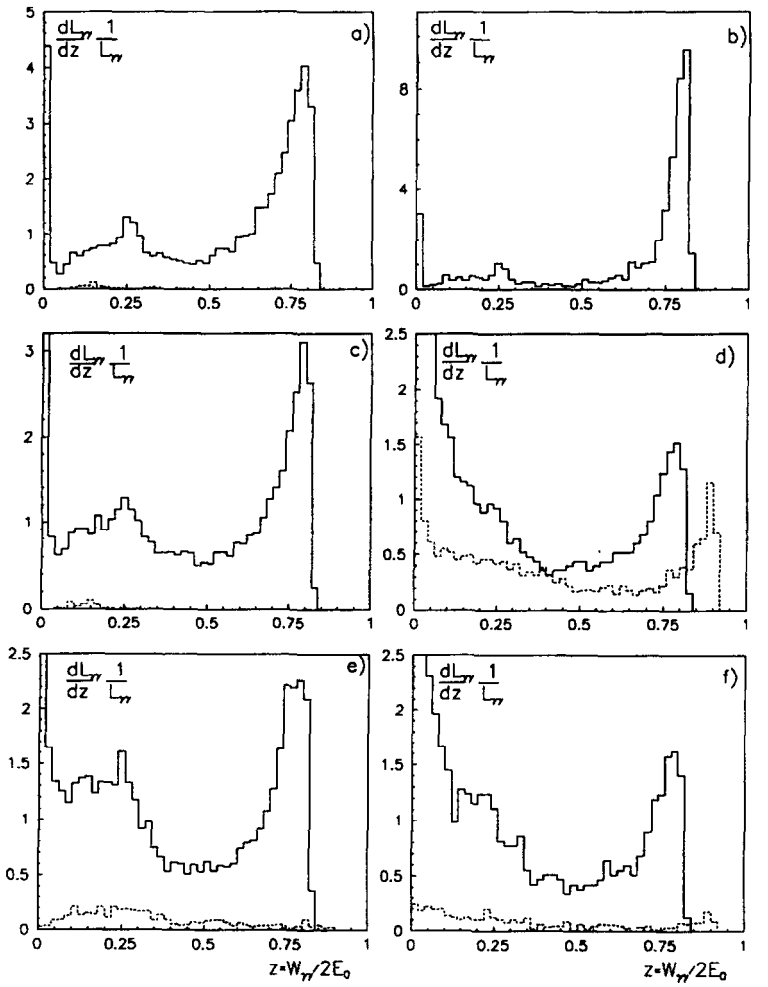

Fig. 12. Spectral luminosities for $\gamma\gamma$ collisions obtained by simulation taking into account main effects at conversion and interaction regions. Dashed histogram is γe luminosity normalized to $\gamma\gamma$ luminosity. Parameters of the beams and other results are presented in Table 8.

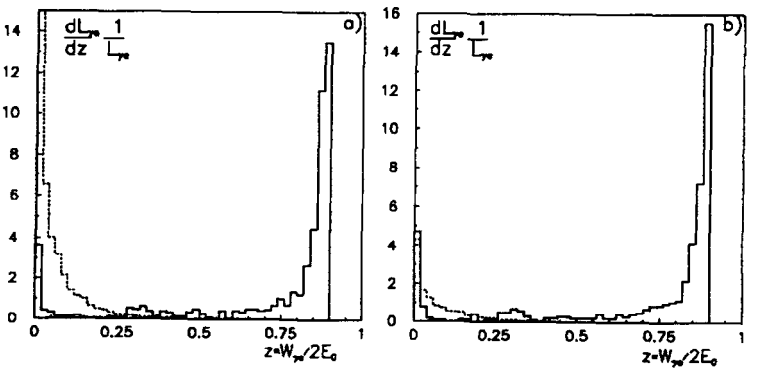

Fig. 13. Spectral luminosities for γe collisions obtained by simulation taking into account main effects at conversion and interaction regions. Dashed histogram is $\gamma\gamma$ luminosity normalized to γe luminosity. Parameters of the beams and other results are presented in Table 8.

ization of the electrons does not change in Compton scattering.

2) Deflection by an external magnetic field and synchrotron radiation in the region between the conversion region and the i.p.

3) Electromagnatic forces, coherent pair creation and beamstrahlung at the i.p.

Beams are composed of about 1000 macroparticles (strings of $0.3\sigma_x$ length). As output the program simulates luminosity spectra, energies and angles of final particles. The results are presented in Table 8 and in Figs. 12 and 13. The dashed histograms in the figures represent the γe and $\gamma\gamma$ background to $\gamma\gamma$, γe collisions respectively.

The considered cases have the following distinct features:

Fig. 12a: $\gamma\gamma$ round electron beams with $\sigma_x = \sigma_y = b/\gamma$, deflection by external field;

Fig. 12b: as Fig. 12a but $\sigma_x = \sigma_y = 0.3b/\gamma$;

Fig. 12c: $\gamma\gamma$ flat beams, $\sigma_y = 0.5b/\gamma$, horizontal deflection;

Fig. 12d: $\gamma\gamma$ flat beams, small b, no deflection;

Fig. 12e: as Fig. 12d but with vertical deflection;

Fig. 12f: $\gamma\gamma$ [26]: $2E_0 = 200$ GeV, flat beams, very large N, no deflection;

Fig. 13a: γe with deflection, $N = 5 \times 10^{10}$;

Fig. 13b: γe with deflection, $N = 10^{10}$.

Some comments on the results shown in Figs. 12 and 13:

1) The wide enhancement around $z = 0.25$ in Figs. 12a–12c is due to collisions with soft photons that occurred in the multiple Compton scatterings.

2) In Fig. 12d there is a very large γe background; it is substantially suppressed in Fig. 12e where vertical magnetic deflection is used.

3) The collider corresponding to Fig. 12f produces fantastic $\gamma\gamma$ luminosity, but disruption angles are large and the number of reactions $\gamma\gamma \rightarrow$ hadrons per beam crossing is 300!

4) The γe luminosity in Fig. 13 at low z is due to collisions of Compton photons with beamstrahlung photons. The low energy $\gamma\gamma$ luminosity is produced by soft photons created in multiple Compton scatterings and beamstrahlung photons.

Other observations and conclusions can be made by the reader, analyzing Table 8 and Figs. 12, 13.

7. Interaction region

A sketch of a possible set-up around the i.p. is shown in Fig. 14. As in e^+e^- colliders, in a photon collider beams are supposed to collide using a "crab crossing" scheme [33], so that after the collision the disrupted beams travel outside lenses. The electron beams in this scheme are tilted with respect to the beam direction at some angle α_c equal to half of the crossing angle so that the luminosity is the same as in head-on collisions. The characterictic disruption angles for a photon colliders are about 10 mrad (see Table 8), but can reach 60 mrad for a 200 GeV collider with superluminosity (case f)).

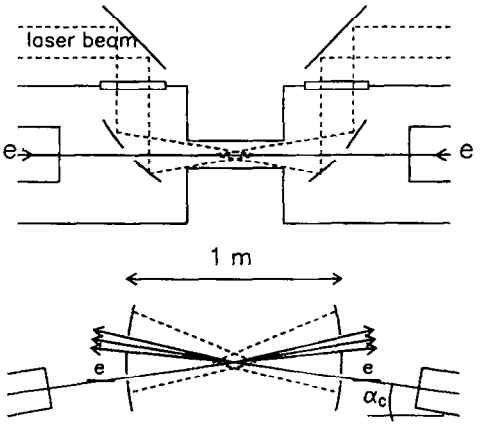

Fig. 14. A schematic layout of the interaction region in a photon collider.

A very powerful laser is focused near to the i.p. To obtain maximum conversion probability the focusing mirrors should be placed at zero angles. In this case they should have holes for passing the initial electron beams and for removal of the highly disrupted beams from the i.p. The angular divergence of the laser light (see Eq. (20)) is

$$\alpha_\gamma > \sqrt{\frac{\lambda}{\pi l_e}} \sim 0.02. \tag{54}$$

Mirrors can reflect a flux of about 1 J/cm^2 in ps region without damage. From the equation

$$A/\mathrm{cm}^2 \sim \frac{3\ \mathrm{J}}{\pi\left(F\alpha_\gamma\right)^2} \sim 1\ \mathrm{J/cm}^2 \tag{55}$$

we find a focal distance $F \sim 50$ cm.

In the scheme with magnetic deflection of the converted electrons a small thin magnet with the field of 10–30 kG should be placed near the i.p. This problem was discussed at this Workshop [17] and needs a further study.

8. Measurement of $\gamma\gamma$ luminosity

A system produced in a $\gamma\gamma$ collision is characterized by its invariant mass $W_{\gamma\gamma} = \sqrt{4\omega_1\omega_2}$ and rapidity $\eta = 0.5 \ln(\omega_1/\omega_2)$. We should have a method to measure 1) $\mathrm{d}^2L/\mathrm{d}W\mathrm{d}\eta$ and 2) $\lambda_{\gamma 1}\lambda_{\gamma 2}$ or, in other words, $\mathrm{d}L_0/\mathrm{d}W\mathrm{d}\eta$ and $\mathrm{d}L_2/\mathrm{d}W\mathrm{d}\eta$ (0, 2–total helicity of the system). These can be measured using the process $\gamma\gamma \rightarrow e^+e^-$[34]. The cross section of this process can be found elsewhere [16,35].

When $\beta \to 1$, then $\sigma_0/\sigma_2 \sim m^2/s$ (excluding the region of small angles). Therefore, the measurement of this process will give us $dL_2/dzd\eta$. How to measure $dL_0/dzd\eta$? This can be done by inversion of the helicity (λ_γ) of the one photon beam by means of changing simultaneously the signs of the helicities of the laser beam used for $e \to \gamma$ conversion and that of the electron beam. In this case the spectrum of scattered photons does not change while the product $\lambda_{\gamma 1}\lambda_{\gamma 2}$ changes its sign. In other words, what was before L_0 is now L_2, which we can measure. The cross section for this process $\sigma(|\cos\Theta| < 0.9) \approx 10^{-36}/s[TeV^2]$ cm^2. This process is very easy to select due to a zero coplanarity angle.

Instead of e^+e^- pairs, muon pairs also can be used [36]. They have the same properties and cross sections. I suggested in Ref. [34] to use e^+e^- pairs only because at high energies the energy of the electrons can be measured much better (using a calorimeter) and easier than for muons.

9. Luminosity and hadronic background

In designs of linear colliders a luminosity of

$$L = 10^{34}\left(\frac{E_{cm}}{1\ \text{TeV}}\right)^2 \text{cm}^{-2}\text{s}^{-1} \qquad (56)$$

is usually assumed as a reference point. In the current designs the effective collision rate is 10^3–10^4/s. It is achieved by using bunch trains of order $n_b \sim 100$ bunches (see Table 1). In NLC, for example, the bunch spacing is only 1.4 ns and it is not simple to distinguished each crossing in time. Let us assume that it is possible and take as a reference a luminosity/crossing about 10^{30} cm^{-2}s^{-1}.

One of the potential problems for photons colliders is hadronic background. At the investigated energies $\sigma(\gamma\gamma \to \text{hadrons}) \approx 300$ nb and it is expected to be about 500 nb at TeV energies. At reference $L/\text{coll} = 10^{30}$ we get 0.5 event/crossing. In general, particles in this process have small $p_\perp$, but hard QCD processes also contribute to the total cross section. The analysis of this problem [37,38] shows that this background is not very serious at such a luminosity per collision. However, it seems rather problematic to work at luminosity 10^{33}/collisions [26]. The analysis of collision effects given in previous sections shows that $L = 10^{30}$/crossing is not a limit for photon colliders. What the limit imposed by hadronic background is, is not yet clear and further analysis is required.

10. Physics (some examples)

The number of papers on physics at γe, $\gamma\gamma$ colliders is growing exponentially in the last three years, proving that the physics is very rich and interesting here and in many respects is complimentary to that in e^+e^- collisions. In these proceedings one can find the detailed analysis of physics at photon colliders. Below one can find a list of some reactions, which are obviously very interesting:

$\gamma e \to W\nu$;

$\gamma e \to Z^0 e$;

$\gamma e \to e^* \to \gamma e$;

$\gamma e \to \tilde{\gamma}\tilde{e} \to \tilde{\gamma}\tilde{\gamma}e$;

$\gamma\gamma \to W^+W^-$;

$\gamma\gamma \to H^+H^-$;

$\gamma\gamma \to L^+L^-$;

$\gamma\gamma \to H^0$.

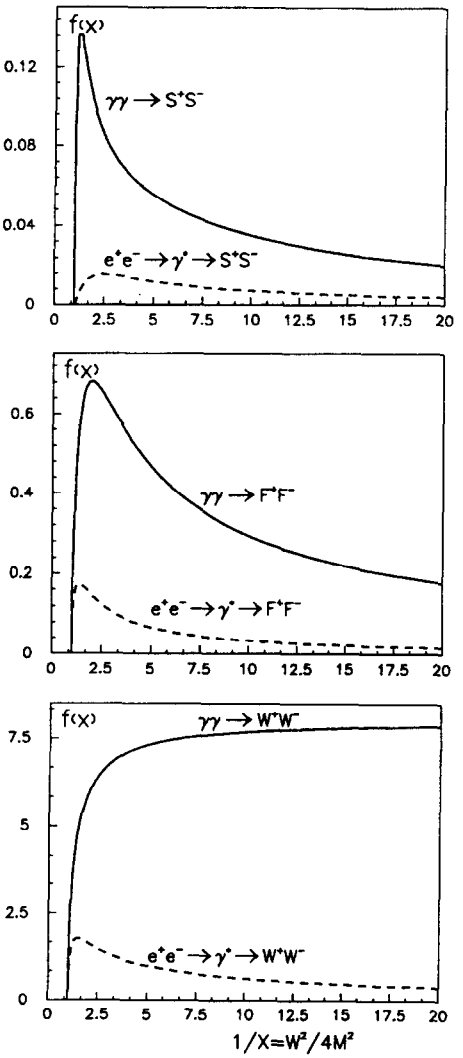

Fig. 15. Comparison of cross sections for charged pair production in e^+e^- and $\gamma\gamma$ collisions. The cross section $\sigma = (\pi\alpha^2/M^2)f_p(x)$; p = S (scalars), F (fermions), W (W-bosons); M is particle mass; $x = W^2_{p\bar{p}}/4M^2$, $f_p(x)$ are shown.

Photon colliders are a factory of Z^0 and $W^{\pm}$ bosons and their properties and interactions can be studied here very well.

In γe collisions one can produce a supersymmetric particle almost twice heavier than in e^+e^- collisions, because the partner is a light particle.

In $\gamma\gamma$ collisions a resonance Higgs production is of particular interest [16,10]. SUSY predicts one of the Higgs's with a mass below 130 GeV. Simulation shows it can be studied at photon colliders.

It is remarkable that cross sections for the production of charged pairs in $\gamma\gamma$ collisions are higher than in e^+e^- collisions (see Fig. 15).

Acknowledgements

I would like to thank A. Sessler for organizing the First Workshop on Gamma–Gamma Colliders, which I hope will stimulate not only theoretical but experimental works as well. I am very grateful to I. Ginzburg, G. Kotkin, V. Serbo, and P. Chen for joint work and to V. Balakin, D. Burke, D. Cline, K. Geissler, W. Kozanecki, D. Meyerhofer, D. Miller, V. Parkhomchuk, B. Palmer, F. Richard, J. Spenser, A. Skrinsky, and W. Vernon for useful discussions.

References

[1] I. Ginzburg, G. Kotkin, V. Serbo and V. Telnov, Pizma ZhETF 34 (1981) 514; JETP Lett. 34 (1982) 491 (Preprint INF 81-50, Novosibirsk (1981) in English).
[2] C. Akerlof, Preprint UMHE 81-59, Univ. of Michigan (1981).
[3] I. Ginzburg, G. Kotkin, V. Serbo and V. Telnov, Nucl. Instr. and Meth. 205 (1983) 47 (Preprint INP 81-92, Novosibirsk (1981) in English).
[4] V. Balakin and A. Skrinsky, Preprint INF 81-129, Novosibirsk (1981); A. Skrinsky, Uspekhi Fiz. Nauk 138 (1982) 3.
[5] A. Kondratenko, E. Pakhtusova and E. Saldin, Dokl. Akad. Nauk 264 (1982) 849.
[6] I. Ginzburg, G. Kotkin, S. Panfil, V. Serbo and V. Telnov, Nucl. Instr. and Meth. 219 (1984) 5.
[7] V. Telnov, Nucl. Instr. and Meth. A 294 (1990) 72.
[8] V. Telnov, Proc. Workshop on Physics and Experiments with Linear Colliders, Lapland, Finland, September 9–14, 1991.
[9] F.R. Arutyunian and V.A. Tumanian, Phys. Lett. 4 (1963) 176;
R.H. Milburn, Phys. Rev. Lett. 10 (1963) 75.
[10] D. Borden, D. Bauer and D. Caldwell, SLAC-PUB-5715, UCSD-HEP-92-01.
[11] Proc. 9th Int. Workshop on Photon–Photon Collisions, San Diego, 1992 (World Scientific).
[12] Proc. Workshop on Physics and Experiments at Linear Colliders, Hawaii, 1993.
[13] I.F. Ginzburg, Proc. 9th Int. Workshop on Photon–Photon Collisions, San Diego 1992 (World Scientific).
[14] S. Brodsky, Proc. Workshop on Physics and Experiments at Linear Colliders, Hawaii, 1993 (World Scientific).
[15] G. Low and B. Wiik, Proc. 5th Workshop on Next Linear Colliders, SLAC, Stanford, Oct. 1993, SLAC-436.
[16] T. Barklow, SLAC-PUB-5364 (1990).
[17] F. Richard, these Proceedings (Workshop on Gamma–Gamma Colliders, Berkeley, CA, USA, 1994) Nucl. Instr. and Meth. A 355 (1995) 92.
[18] L. Landau and E. Lifshitzs, Kvantovaya mekhanika, vol. 1, (M. Nauka).
[19] I. Ginzburg, G. Kotkin and S. Polityko, Yad. Fizika 40 (1984) 1495; 37 (1983) 368.
[20] K. Geissler, presented at the Workshop on Physics and Experiments with Linear Colliders, 1991, Lapland, Finland, unpublished;
See also Ref. [8];
Talk at ECFA Workshop on e^+e^- Linear Colliders, LC92, Garmish-Partenkirchen, 1992, unpublished.
[21] D. Meyerhofer, these Proceedings (Workshop on Gamma–Gamma Colliders, Berkeley, CA, USA, 1994) Nucl. Instr. and Meth. A 355 (1995) 113.
[22] E. Saldin et al., Proc, and Workshop on Physics at VLEPP, Protvino, 2–4 June 1992, vol. 2, p. 96.
[23] A. Sessler, presented at the Workshop on e^+e^- Linear Collisers, Garmish-Partenkirchen, July 1992, unpublished.
[24] E. Saldin, V. Sarantsev, E. Schneidmiller and M. Yurkov, these Proceedings (Workshop on Gamma–Gamma Colliders, Berkeley, CA, USA, 1994) Nucl. Instr. and Meth. A 355 (1995) 171.
[25] S. Hiramatsu et al., ibid., p. 133.
[26] V. Balakin and A.A. Sery, ibid., p. 157.
[27] S. Rajagopalan, D. Cline and P. Chen, ibid., p. 169.
[28] T. Erber, Rev. Mod. Phys. 38 (1966) 626.
[29] P. Chen and V. Telnov, Phys. Rev. Lett. 63 (1989) 1796.
[30] R. Noble, Nucl. Instr. and Meth. A 256 (1987) 427 and references therein.
[31] U. Amaldi, CERN-EP/87–169, Lecture at US-CERN School on Particle Accelerators, South Padre, Texas, 1986.
[32] V. Balakin and N. Solyak, Preprint INF 82–123, Novosibirsk (1982); Proc. 8th All Union Workshop on Char. Particle Accelerators Dubna, 1983, vol. II, p. 263; Proc. 8th Int. Conf. on High Energy Accelerators, Novosibirsk, 1987, p. 151.
[33] R. Palmer, SLAC-PUB 4707 (1988).
[34] V.I. Telnov, Proc. Workshop on Physics and Experiments at Linear Colliders, Hawaii, 1993 (World Scientific).
[35] K. Ispirian et al., Yad. Fiz. 11 (1970) 1278; Sov. J. Nucl. Phys. 11 (1970) 712.
[36] D. Miller, these Proceedings (Workshop on Gamma–Gamma Colliders, Berkeley CA, USA, 1994) Nucl. Instr. and Meth. A 355 (1995) 101.
[37] T. Barklow, P. Chen and M. Peskin, Proc. Workshop on Physics and Experiments at Linear Colliders, Hawaii, 1993 (World Scientific).
[38] P. Chen et al., these Proceedings (Workshop on Gamma–Gamma Colliders, Berkeley, CA, USA, 1994) Nucl. Instr. and Meth. A 355 (1995) 107.